IN PROCEEDINGS OF THE IEEE 2006 INTERNATIONAL CONFERENCE ON
INTELLIGENT ROBOTS AND SYSTEMS (IROS) . BEIJING, CHINA, OCT 9-15 2006


# Dynamical Systems Approach for the Autonomous Avoidance of Obstacles and Joint-limits for an Redundant Robot Arm

Ioannis Iossifidis Institut für Neuroinformatik
Ruhr-Universität Bochum
44801 Bochum, Germany
Email: iossifidis@neuroinformatik.rub.de Gregor Schöner Institut für Neuroinformatik
Ruhr-Universität Bochum
44801 Bochum, Germany
Email: gregor.schoener@neuroinformatik.rub.de

***Abstract*— We extend the attractor dynamics approach to generate goal-directed movement of a redundant, anthropomorphic arm while avoiding dynamic obstacles and respecting joint limits. To make the robot's movements human-like, we generate approximately straight-line trajectories by using two heading direction angles of the tool-point quite analogously to how movement is represented in the primate central nervous system. Two additional angles control the tool's spatial orientation so that it follows the tool-point's collision-free path. A fifth equation governs the redundancy angle, which controls the elevation of the elbow so as to avoid obstacles and respect joint limits. These variables make it possible to generate movement while sitting in an attractor (or, in the langauge of the potential field approach, in a minimum). We demonstrate the approach on an assistant robot [1], which interacts with human users in a shared workspace.**

## I. Introduction

Enabling autonomous robots to act in natural environments while interacting with human users continues to be a major challenge. One of the most basic tasks for such systems is to manipulate objects in a workspace shared with the human user. The task requires the simultaneous satisfaction of multiple constraints that include moving toward appropriate grasping configurations, avoiding dynamical obstacles, avoiding joint-limits, and reacting to unexpected changes in the scene. People can do that effortlessly, of course, and some of their motor control strategies may serve as a source of inspiration for the engineer.

The robotic assistant CoRA (see fig. 1) is designed to interact with humans through a number of interaction channels (speech, gesture-recognition, artificial skin) in a shared workspace analyzed by a stereo-camera system [2], [3]. CoRA's anthropomorphic geometry was chosen so that its arm movements would be human-like. This makes the arm's movement predictable for the human operator, a very important feature if people are to collaborate effortlessly with the robotic assistant in such settings as help for the elderly or handicapped, or in the household.

Human arm movement is characterized by approximately straight-line paths of the tool-point movement goals (e.g., [4]). In prior work we have used the direction in space of the end-effector variable to generate such human-like movement paths [1]. Our method was based on the attractor dynamics approach, orginally developed to plan and control vehicle motion [5], [6], [7]. In its simplest form, the attractor dynamics approach is a mathematically formalized variant of the potential field method. By using heading direction rather than the cartesian position of the vehicle, the movement plan is generated while the planning variable is sitting in the minimum (the attractor), not through the transient down-hill solution as in the conventional potential field approach [8], [9]. The advantage of using heading direction has been described earlier in [10] as a simple way to avoid some of the problems of the potential field methods like spurious minima and oscillations (e.g., [11]), without incurring the large compuational cost of exact solutions (e.g., [12]). Based on bifurcation theory [13], the attractor dynamics formulation makes it possible to control and design decision making in the presence of multiple minima. As a result, the movement plan maintains temporal continuity, a property particularly important in the higher-dimensional problems of motion control in robot arms.

To generalize the attractor dynamics approach to the control of a robot arm, two angles of heading direction were used. These control the direction in three dimensional space in which the tool-point moves [1]. (Incidently, in the nervous system of primates, it is the direction in space of the end-effector path that is represented in the relevant cortical areas by populations of neurons [14]). The result is a very simple method, based on two equations, into which the target enters as an attractive force and the obstacles enter as repulsive forces, and which generates collission-free paths of the end-effector. Impedence control [15] is a related, sophisticated method that generates motion on the basis of constraints on the end-effector. The attractor dynamics approach is, by comparison, much simpler, does not require estimation and control of forces or torques but is limited to kinematics. Multi-point impedance control for redundant manipulators [16] extends the impedance control approach to constraints for the entire robot arm. The present paper makes the analogous move for our simpler,

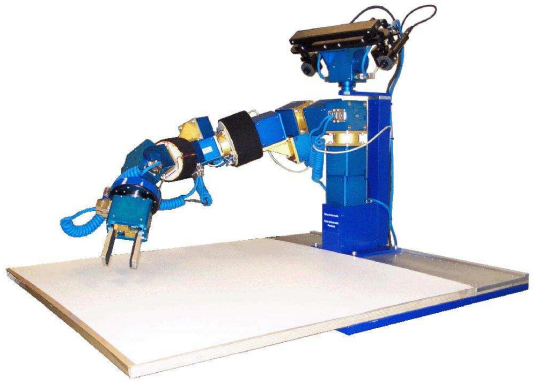

Fig. 1. The anthropomorphic robotic assistant CORA.

kinematic attractor dynamics approach, which we generalize to include dynamic collision-avoidance of the arm itself and the consideration of joint limits. The approach is heuristic and makes use of a number of simplifying assumptions, but is considerably simpler than more general methods (e.g., [17]) and maintains the human-like movement trajectories.

One simplification arises from the scenario we are addressing: The human user and the robot arm reach for objects on a table surface (Fig. 1). The robot arm avoids all obstacles, be they objects positioned on the table or body parts of the human operator by moving above the occupied regions in space, never by moving below the the occupied space (e.g., never in the space between the table and the human operator).

The idea then is to backtrack the movement plan from the distal to the proximal segments: The tool-point trajectory is generated through two heading-directions. We control the arm such that the wrist and forearm follow the collision-free path in space on which the end-effector has moved. We then exploit the redundancy of the arm in order to control the spatial position of the elbow both to clear obstacles with the upper arm and to satisfy joint-limit constraints at the wrist. All constraints are integrated by adding forces to attractor dynamics equations for the hand orientation in space and for the redundancy angle, which controls elbow elevation.

We first briefly review the kinematics of the redundant, anthropomorphic arm, defining the redundancy angle and linking it to the two constraints of obstacle avoidance and joint limits. Then we describe the total of five dynamical systems equations from which the arm trajectory is obtained as an attractor solution, the system sitting at all times in the attractor. Finally, we describe the implementation of this approach on the robotic assistant CORA and illustrate its performance.

## II. KINEMATICS

### A. Inverse kinematics

The reference arm configuration is show in Figure 2. The arm is composed of a series of *roll* and *pitch* joints. The combination of a *roll-pitch-roll*-joint is functionally equivalent to a spherical three DoF joint like the human shoulder or wrist.

The trunk of the robot is controlled separately by generating a constant joint velocity that brings the shoulder girdle

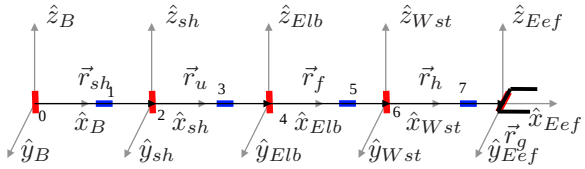


Fig. 2. Initial Arm Configuration and coordinate systems:

from its initial position to an orientation perpendicular to the direction from the base of the torso to the target position. This orientation of the shoulder has been found to be best suited for grasping (not unlike the position spontaneously adopted by humans when they make manipulation movements).

The inverse kinematics problem for the remaining seven degrees of freedom is solved in closed form [18][19]. Given the hand orientation $\theta_{EEF}$ (elevation) and $\phi_{EEF}$ (azimuth) and the hand reference point, the vector $\vec{r}_h$ from the wrist to the hand reference tool-point (Fig. 3) is determined as

$$\vec{r_h} = \mathcal{R}_z^{\phi_{EEF}} \cdot \mathcal{R}_y^{\theta_{EEF}} \cdot \hat{e}_x \cdot l_h \tag{1}$$

where $\mathcal{R}_x$, $\mathcal{R}_z$ denote rotation matrices around the z- and y-axes, $\hat{e}_x$ the unit vector in the $x$-direction and $l_h$ denotes the seqment length.

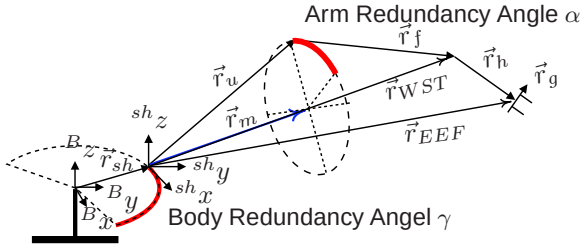


Fig. 3. The redundancy of the shoulder and the elbow joints

The redundant degree of freedom is defined by the *redundancy circle*, the center $\vec{r}_m$

$$\vec{r}_m = \frac{|\vec{r}_u|^2 - |\vec{r}_f|^2 + |\vec{r}_{WST}|^2}{2 \cdot |\vec{r}_{WST}|^2} \vec{r}_{WST} \tag{2}$$

of which lies on a ray pointing from the shoulder to the wrist joint. The spatial position of the elbow lies on this circle of radius $R$:

$$R = \sqrt{|\vec{r}_u|^2 - \left( \frac{|\vec{r}_u|^2 - |\vec{r}_f|^2 + |\vec{r}_{WST}|^2}{2 \cdot |\vec{r}_{WST}|} \right)^2} \tag{3}$$

Expressing the wrist vector, $\vec{r}_{WST}$, through two angles, $\phi_{WST}$ and $\theta_{WST}$, the elbow position can be written as

$$\vec{r}_u = \left( \mathcal{R}_x^{\phi_{WST}} \mathcal{R}_z^{\theta_{WST}} \mathcal{R}_x^{\alpha} \cdot \hat{e} \right) \cdot R + \vec{r}_m \tag{4}$$

where $\mathcal{R}_x$ and $\mathcal{R}_z$ are rotation matrices around the x- and the z-axis and the *redundancy angle*, $\alpha$, characterizes the position of the elbow on the redundancy circle (Fig. 3). If the redundancy angle, $\alpha$, is specified, all limb vectors are known. A straightforward solution of the inverse kinematics determines the joint angles $\theta_1, \theta_2, \theta_3 \theta_4, \theta_5, \theta_6, \theta_7$.

### B. Constraints for the redundancy circle

The redundancy angle $\alpha$ spans all redundant arm configurations consistent with the same tool position and orientation. The rate of change of the redundancy angle generates self-motion, which can be used to accomodate the two additional constraints of obstacle avoidance for the upper arm and joint limits at the wrist. To do that, we must compute which sectors on the redundancy circle are disallowed by these constraints.

Any obstacle, $i$, that reaches up to the elbow, defines a to-be-avoided segment on the redundancy circle centered on $\kappa_{obs,i}$ and with an angular range of $\sigma_{obs,i} = 2 \cdot \delta_o$ (see Fig. 4)

Transforming limitations of joint angle range into constraints on the redundancy circle is more complicated. The most important joint angle limitation concerns the wrist, where the lower arm and the hand are spatially aligned. The angle, $\mu$, between the hand $\vec{r}_h$ and the forearm $\vec{r}_f$ must larger than $\pi/2$, which is true as long as

$$-(\pi - \mu) \leq \theta_6 \leq \pi - \mu \tag{5}$$

where $\theta_6$ is the joint angle of the sixth robot arm module (see Fig. 2). Fig. 4 illustrates that this can be used to compute the corresponding allowable sector on the redudancy circle. To do

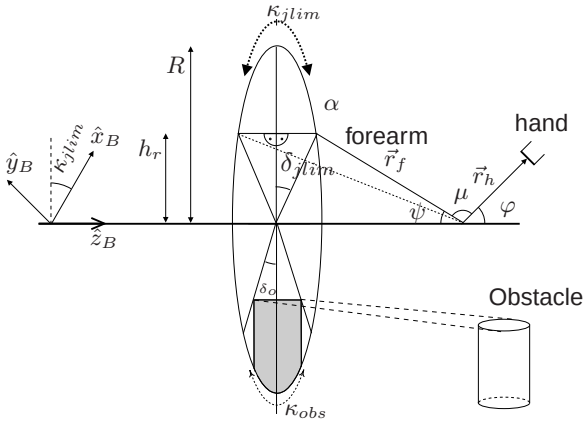


Fig. 4. Geometrical construction to avoid joint configurations at the wrist and an obstacle reaching into the redundancy circle defines a to-be-avoided angular segment of that circle.

that, define a coordinate system $(x_B, y_B, z_B)$ of which the $z_B$-axis is aligned with the shoulder-wrist-axis of the robot arm. If $\phi_{EEF}$ and $\theta_{EEF}$ describe the azimuth and elevation of the wrist, then the transformed hand vector, $\vec{r}_h'$ is:

$$\vec{r}_h' = \mathcal{R}_y^{-\theta_{EEF}} \mathcal{R}_z^{-\phi_{EEF}} \cdot \vec{r}_h \tag{6}$$

After the transformation, the redundancy circle lies in a plane parallel to the $x' - y'$-plane, so that we may project $\vec{r}_h'$ onto the $x' - y'$-plane to obtain:

$$\kappa = \arctan(r_h^{y\prime}, r_h^{x\prime}) \tag{7}$$

as the center of the prohibited sector of the redundancy circle. The angular extent of the prohibited region $\kappa \pm \delta$ follows from Eq. 5:

$$\delta_{jlim} = \arccos(h_r / R) \tag{8}$$

where $h_r$, $\psi$, $c$ and $\varphi$ are auxiliary quantities, which can be derived from figure 4:

$$h_r = c \cdot \tan(\psi) \tag{9}$$

$$c = |\vec{r}_{EEF}| - |\vec{r}_m| \tag{10}$$

$$\psi = \mu - \varphi \tag{11}$$

$$\varphi = \arccos\left(r_h^{z\prime} / |\vec{r}_h'|\right) \tag{12}$$

## III. Attractor dynamics of arm motion

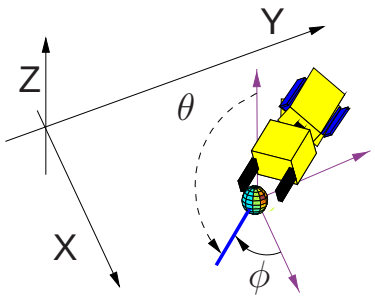


Fig. 5. The end-effector position (sphere) is shown in a world coordinate frame fixed to the working surface ($z = 0$). The instantaneous heading direction of the end-effector is represented by two angles relative to the vertical world axis (elevation, $\theta$) and the world x-axis (azimuth, $\phi$).

### A. Attractor dynamics of end-effector motion

Three *behavioral variables* [6] are used to generate the movement trajectories of the 3D position of the end-effector of the robot arm. Two heading direction angles are illustrated in Figure 5. These may be defined using spherical coordinates of a coordinate frame that is attached to the end-effector, but remains aligned relative to an arbitrary, but fixed world reference frame. The elevation, $\theta$, is the angle between the direction in which the end-effector is moving and the vertical axis. The azimuth, $\phi$, is the angle between the projection of the direction in which the end-effector is moving onto the meridional plane and the arbitrary, but fixed x-axis of the world coordinate frame. The third variable is the path velocity, which is kept constant during movement.

The planned trajectory is characterized by the time courses of these two heading angles, $\theta(t)$ and $\phi(t)$. These time courses are generated by solving a dynamical system

$$\tau\dot{\phi}(t) = f_{\text{tar}}(\phi) + \sum_i f_{\text{obs},i}(\phi, \phi_i) \tag{13}$$

$$\tau\dot{\theta}(t) = g_{\text{tar}}(\theta) + \sum_i g_{\text{obs},i}(\theta, \theta_i) \tag{14}$$

built from components that generate target acquisition ($f_{\text{tar}}$ and $g_{\text{tar}}$) and avoidance of a discrete set of obstacles ($f_{\text{obs},i}$ and $g_{\text{obs},i}$). The parameter, $\tau$, fixes the units of time.

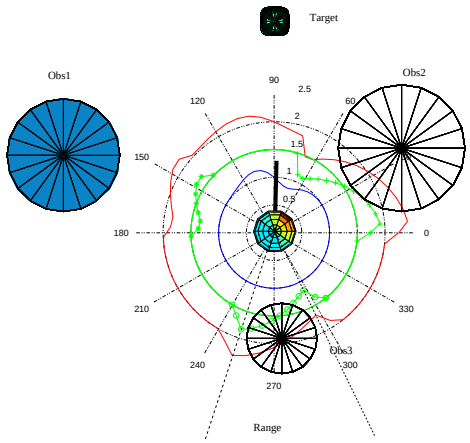


Fig. 6. Target acquisition and obstacle avoidance. Depicted is the phaseplot of the dynamical system concerning the contribution of three obstacles and one target in polar coordinates with $\dot{\phi} = r(\phi)$. The target is specifying an attractor (negative slope) and obstacles are specifying repellors.

*1) Target acquisition:* From the scene analysis, an estimate of the Cartesian position, $(x_{\rm tar}, y_{\rm tar}, z_{\rm tar})$, of the target in the world frame is obtained. The 3D position of the end-effector, $(x, y, z)$, is upated continously. Together, these two positions defined the angles, $\phi_{\rm tar}$ and $\theta_{\rm tar}$ under which the end-effector sees the target. The target contributions to the dynamics of heading direction are sinusoidal forces (to respect the angular nature of the variables (see also Fig. 6)):

$$f_{\rm tar}(\phi) = \lambda_{\rm tar} \sin(\phi - \phi_{\rm tar}) \quad (15)$$
$$g_{\rm tar}(\theta) = \lambda_{\rm tar} \sin(\theta - \theta_{\rm tar}). \quad (16)$$

The parameter $\lambda_{\rm tar}$ determines the strength of attraction toward the target and must be small relative to the obstacle contributions.

*2) Obstacle avoidance:* Sensory information must provide for each obstacle $(i)$ estimates of its position on the working surface $(x_i, y_i)$, its maximal height, $h_i$, and the radius, $r_i$, of a circle enclosing its footprint. For the azimuthal heading direction, obstacle avoidance is implemented strictly analogously to how it is done for vehicles. The angle,

$$\phi_i = \arctan\left((y_i - y)/(x_i - x)\right) \quad (17)$$

under which the base of the obstacle in the working surface is seen from the point of view of the end-effector, repels the azimuthal heading direction.

The function

$$f_{{\rm obs},i}(\phi) = \lambda_{\rm obs} \cdot \sin(\phi - \phi_i) \cdot \exp\left[-\frac{(\phi - \phi_i)^2}{2\sigma^2}\right] \cdot \exp(-d_i/d_0) \cdot \text{range}(\phi - \phi_i, d_i). \quad (18)$$

generates a repulsive force with limited angular range, so that an obstacle affects the path only as long as the end-effector is moving toward the obstacle. The repulsion strength, $\lambda_{\rm obs}$, is a function of the minimal distance $d_i$ between end-effector and obstacle, so that an obstacles becomes repulsive only when the end-effector comes sufficiently close as scaled by the parameter, $d_0$. The angular range is determined by the angle, $\Delta\phi_i$, under which the footprint of the obstacle is seen from the end-effector position (and which again depends on the distance, $d_i$, to the obstacle) augmented by a safety margin, $\delta_m$:

$$\text{range}(\phi - \phi_i, d_i) = \frac{1}{2}[\tanh(\beta \cdot (\cos(\phi - \phi_i) - \cos(2\Delta\phi(d_i) + \delta_m)) + 1] \quad (19)$$

where $\beta$ is a model parameter determining how sharply the range function declines. The sharp cut-off of this function at the boundaries of the obstacle is smoothed via the Gaussian function (width parameter, $\sigma$). For a more detailed description see [1].

### B. Attractor dynamics of hand orientation

The goal is now to keep the hand aligned with the tangent to the end-effector path, so that the hand moves through the collision-free path generated for the end-effector. That tangent to the end-effector trajectory is approximated by:

$$s_T(t) = \vec{r}(t_n) - \vec{r}(t_{n-1})/|\vec{r}(t_n) - \vec{r}(t_{n-1})| \quad (20)$$

Transforming this vector into spherical coordinates yields two angles, $\varphi_{s_T}$ and $\vartheta_{s_T}$, which will vary in time as the movement unfolds. The hand orientation can be controlled by defining a dynamics with these two angles as moving attractors:

$$\dot{\phi}_{WST} = \lambda_{tar} \sin(\phi_{WST} - \varphi_{s_T}) \quad (21)$$
$$\dot{\theta}_{WST} = \lambda_{tar} \sin(\theta_{WST} - \vartheta_{s_T}) \quad (22)$$

### C. Attractor dynamics of elbow motion

Finally, yet another dynamical system generates the time course of the redundancy angle, $\alpha(t)$. This systems is built as a sum of individual contributions:

$$\dot{\alpha} = h_{\rm tar}(\alpha) + \sum_i h_{{\rm obs},i}(\alpha, \alpha_i) + \sum_i h_{{\rm jlim},i}(\alpha, \alpha_i)$$

that express the contraints of obstacles avoidance $(h_{{\rm obs},i}(\alpha, \alpha_i))$ and of joint limits $h_{{\rm jlim},i}(\alpha, \alpha_i)$. The "target" contribution sets an attractor at a preferred, default elbow configuration through

$$h_{\rm tar}(\alpha) = \lambda_{tar} \sin(\alpha - \alpha_{tar}) \quad (23)$$

Obstacle avoidance consists of a "force-let" that repels from the centers, $\kappa_{obs,i}$, of the prohibited segments on the redundancy circle with a range, $\sigma_{obs,i}$ (cf. section II-B)

$$h_{obs,i}(\alpha) = \lambda_{obs} \cdot \sin(\alpha - \kappa_{obs,i}) \cdot \exp\left(-\frac{(\alpha - \kappa_{obs,i})^2}{2\sigma_{obs,i}^2}\right) \cdot \exp\left(-\frac{d_i}{d_o}\right) \quad (24)$$

where the strength of repulsion $\lambda_{obs}$ is a decreasing function of the minimal distance between the robot arm and the obstacle. This distance is computed based on a cylindrical obstacle model as well as a cylindrical segment model of the robot arm.

The repulsive "force-let" representing joint limit restrictions is defined as:

$$h_{jlim}(\alpha) = \lambda_{jlim} \cdot \sin(\alpha - \kappa_{jlim}) \cdot \exp\left(-\frac{(\alpha - \kappa_i)^2}{2\sigma_{jlim,i}^2}\right) \quad (25)$$

where $\sigma_{jlim,i} = 2 * \delta_{jlim}$ (see section II-B and Fig. 4).

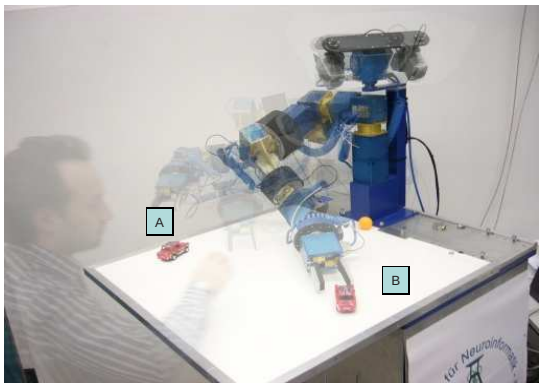


Fig. 7. The robot arm tracks a target which is displaced by the human operator during arm movement

## IV. Implementation

### A. Anthropomorphic robot CoRA

CoRA (Figure 1) is custom-built from individual servo-controlled motor modules. Each module has its own control unit and communicates via a CAN-bus interface with the master control PC. A two DoF pan/tilt unit is mounted as a "head" above the torso. It carries a stereo color camera system and two microphones. Computational power for computer vision and other sensory processing is provided by a fast Ethernet network of 5 PCs with 1600Mhz Athlon CPUs running LINUX. Although CoRA possesses vision algorithms that provide target coordinates [2], [3], an estimation of pose, and obstacle information, we have implemented and evaluated the attractor dynamics trajectory generation method in a first step based on obstacle and target data measured externally.

### B. Numerical solution of the dynamics

The set of dynamical systems is solved numerically using a simple Euler algorithm. An updated occurs at each Euler step for: all parameters describing obstacle and target angles, distances, and range functions; the solution of the differential equations; the inverse kinematics evaluated to transform the new end-effector velocity vector into a vector of joint velocities, and new velocity set-points, which are sent to the robot arm joint servos. The new Cartesian position of the end-effector is obtained by applying the forward kinematics to the new joint angle positions. The duration of the Euler step in implementation was measured and the time scale, $\tau$, was chosen sufficiently large for this Euler step to approximate the dynamics.

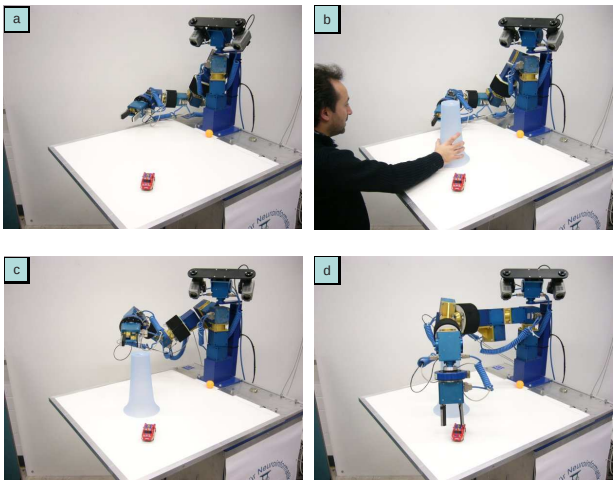


Fig. 8. The system reacts on the sudden occurrence of an obstacle

### C. Results

The new approach enables collision free movement in a considerably wider set of obstacle and target geometries than our earlier method. We systematically varied the layout of the objects on the table to establish that. The following demonstrations illustrate the basic behavioral patterns that support this performance.

*1) Wrist and elbow motion in dynamic environments:* In figure 7 the situation is shown where the robot is moving the end-effector toward a target in a scene without obstacles. During the movement the robots stays in the preferred configuration with a low elbow not unlike how humans would move in this situation. This makes the robot's motion intuitive and predictable for the human partner. It is also faster than any motion that would reconfigure the arm. The system proves its flexibility by tracking the target object which was displaced by the human operator during the arm movement from position A to postion B in figure 7.

In comparison we observe in figure 8 how the presence of an obstacle is forcing the robot arm to leave the preferred configuration by modifying the motion of the wrist and the elbow. While the end-effector is guiding the robot arm above the obstacle (figure 8c ) the hand orientation is following the end-effector path and the elbow is lifted into a safe position (8d). The sudden occurrence of an obstacle, provoked again by the human operator (figure 8), proves the flexible and highly reactive character of this approach.

*2) Cluttered environment:* In the last experiment the performance of the approach is tested in a static environment with higher obstacle density as shown in figure 9. We arranged the scene such that an target is surrounded by three obstacles (a phaseplot of the dynamical system is shown in figure 6). This is the three-dimensional analogue of a u-shaped obstacle with a narrow passage. This scenario should uncover limitations of the approach like the occurrence of spurious minima or oscillations, if they exist.

After initiating the movement towards the target position the repulsive force-let is steering the endeffector over the first obstacle. In figure 9 c) the elbow is lifted into a save position

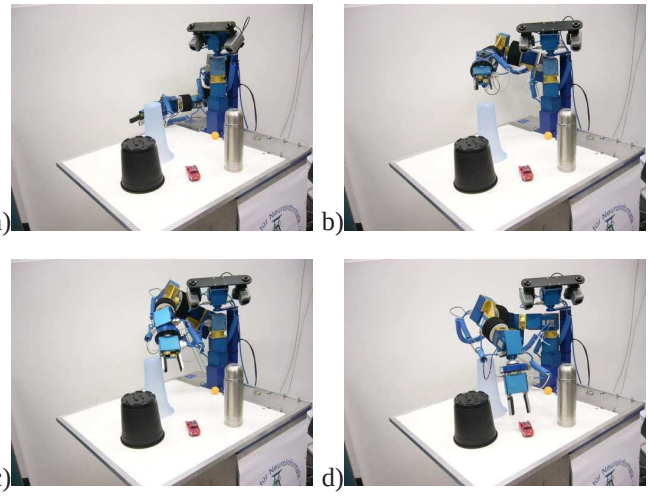


Fig. 9. Arm movement in a cluttered environment

due to the obstacle contribution (see eq. 24). In figure 9 d) the end-effector is diving behind the obstacle in order to reach the target object. The hand orientation is following the end-effector path which leads to an configuration close to the joint angle limit between wrist and forearm. Due to the resulting joint-limit contribution the elbow is lifted higher (comare 9 c) and 9 d)). Finally the end-effector reaches the target object without colliding with the obstacles, getting stuck or starting to oscillate.

## V. Conclusion

The attractor dynamics approach to trajectory formation was generalized to the control of the motion of a redundant robot arm by applying a task decomposition, comprising endeffector, wrist and elbow motion. Propagating the end-effector path backward along the kinematic chain, the collision-free path of the end-effector was exploited to generate obstacle avoidance along the rest of the robot arm. Time courses of the heading-direction of the end-effector, of the elevation and the azimuth angles, were obtained from an attractor dynamics, into which obstacles contributed repulsive force-lets. The elbow motion was driven by an attractor dynamics, into which obstacles and joint limit constraints were coupled as repulsive force-lets as well. We showed that with very simple, low-dimensional scene descriptors, the approach leads to reaching behavior on table tops in the presence of relatively complex obstacle layouts.

The presented approach is a heuristic one, which works only within the limits of how much flexibility the extra degrees of freedom of the arm provide. It is not capable of predicting beforehand if a collision-free path is possible nor is it necessarily capable of always finding such a path even if one exists. A further enhancement consists of predicting the arm path by internal simulation, detecting collisions based on obstacle and arm models. Parameter values can then be adjusted to enhance repulsion from the collision points and a collision-free path be searched interactively. This method has already been tested successfully in simulation. A next step could be to detect collisions while the arm is moving by touch sensors (e.g., using the artificial skin of our CoRA system [3]) and to iteratively adjust parameter values to enhance avoidance. Internal simulation with the adjusted parameter value can predict if the path may reach the goal at all.

## References

[1] I. Iossifidis and G. Schöner, "Autonomous Reaching and Obstacle Avoidance With the Anthropomorphic Arm of a Robotic Assistant Using the Attractor Dynamics Approach," in *Proceedings of the IEEE 2004 International Conference On Robotics and Automation*, New Orleans, USA, April 26 - May 1 2004.

[2] I. Iossifidis, C. Bruckhoff, C. G. C Theis, C. Faubel, and G. Schöner, "CORA: An Anthropomorphic Robot Assistant for Human Environment," in *Proceedings of the 2002 IEEE Int. Workshop on Robot and Human Interactive Communication Berlin, Germany, Sept. 25-27, 2002*, 2002, pp. 392–398.

[3] I. Iossifidis, C. Theis, C. Grote, C. Faubel, and G. Schöner, "Anthropomorphism as a pervasive design concept for a robotic assistant," in *Proceedings of the IROS 2003 IEEE/RSJ International Conference on Intelligent Robots and Systems*, 2003.

[4] D. A. Rosenbaum, *Human Motor Control*. Academic Press, Inc., 1991.

[5] G. Schöner and M. Dose, "A dynamical systems approach to task-level system integration used to plan and control autonomous vehicle motion," *Robotics and Autonomous Systems*, vol. 10, pp. 253–267, 1992.

[6] G. Schöner, M. Dose, and C. Engels, "Dynamics of behavior: Theory and applications for autonomous robot architectures," *Robotics and Autonomous Systems*, vol. 16, pp. 213–245, 1995.

[7] A. Steinhage and G. Schöner, "Dynamical Systems for the Behavioral Organization of Autonomous Robot Navigation," in *Sensor Fusion and Decentralized Control in Robotic Systems: Proceedings of SPIE*, M. G. T. Schenker P S, Ed., vol. 3523, no. ISBN 0-8194-2984-8. SPIE-publishing, 1998, pp. 169–180.

[8] J. R. Andrews and N. Hogan, "Impedance Control as a Framework for Implementing Obstacle Avoidance in a Manipulator," in *Control of Manufacturing Processes and Robotic Systems*, E. E. Hardt and W. Book, Eds. ASME, Boston, 1983, pp. 243–251.

[9] O. Khatib, "Real-time obstacle avoidance for manipulators and mobile robots," *International Journal Robotics Research*, vol. 5, pp. 90–98, 1986.

[10] Y. Koren and J. Borenstein, "Potential Field Methods and Their Inherent Limitations for Mobile Robot Navigation," in *Proceedings of the 1991 IEEE International Conference on Robotics and Automation*, Sacramento, California, 1991, pp. 1398–1404.

[11] A. McLean and S. Cameron, "The virtual springs method: path planning and collision avoidance for redudannt manipulators," *IJRR*, vol. 15, pp. 300–319, 1996.

[12] E. Rimon and D. E. Koditschek, "Exact robot navigation using artificial potential functions," *IEEE Transactions on Robotics and Automation*, vol. 8, no. 5, pp. 501–518, 1992.

[13] L. Perko, *Differential Equations and Dynamical Systems*. Berlin, Germany: Springer-Verlag, 1991.

[14] A. P. Georgopoulos, "Neural aspects of cognitive motor control," *Current Opinion in Neurobiology*, vol. 10, no. 2, pp. . 238–241, 2000.

[15] N. Hogan, "Impedance Control: An Approach to manipulation, Parts I, II, III," *Dynamic System Control*, vol. 107, no. 1, pp. 1–24, 1985.

[16] T. Tsuji, Achmad Jazidie, and Makoto Kaneko, "Multi-Point Impedance Control for Redundant Manipulators," *IEEE Transactions on Systems, Man and Cybernetics*, vol. 26, 5 October 1996.

[17] O. Brock and O. Khatib, "Real-Time Replanning in High-Dimensional Configuration Spaces Using Sets of Homotopic Paths," in *International Conference on Robotics & Automation San Francisco, CA, April 2000*, 2000.

[18] K. Kreutz-Delgado, Long M, and H. Seraji, "Kinematic analysis of 7-DOF manipulators," *IJRR*, vol. 11, pp. 469–481, 1992.

[19] J. M. Hollerbach, "Optimum kinematic design for a seven degree of freedom manipulator," in *Proceedings of Robotics Research: the Second International Symposium*, H. Hanafusa and H. Inoue, Eds. Cambridge, Mass.: MIT Press, 1985, pp. 215–222.